Tuning the surface stabilization of LiNiO$_2$ cathode via mixed conductive carbon nanotube/lithium polyacrylate coatings – Electrochemical performance and operando gas evolution analysis

Rekha Narayan [a], Irina Profatilova [b], Gregor Kapun [a], Elena Tchernychova [a], Elisabeth Addes [b], Robert Dominko [a,c,d,*]

[a] National Institute of Chemistry, Hajdrihova 19, SI-1000, Ljubljana, Slovenia
[b] University Grenoble Alpes, CEA-LITEN, DEHT, 17 ave. Des Martyrs, F-38000, Grenoble, France
[c] Faculty for Chemistry and Chemical Technology, University of Ljubljana, Večna Pot 113, 1000, Ljubljana, Slovenia
[d] Alistore-European Research Institute, CNRS FR 3104, Hub de l'Energie, Rue Baudelocque, 80039, Amiens, France

A B S T R A C T

LiNiO$_2$ (LNO), one of the most promising Ni-rich cathode materials for Li-ion batteries is limited in its practical applicability due to structural and surface degradation. Protective surface coatings are a viable strategy to create a stable interface. In this work, the surface modification of LNO cathode using mixed electron/ion conductive composite coatings based on carboxyl-functionalized multi-walled carbon nanotubes (oMWCNTs) and poly-acrylic acid (PAA) is presented, aiming at an optimal balance of electronic and ionic conductivity, respectively. In-situ conversion reaction of PAA with the detrimental Li residues (Li$_2$CO$_3$, LiOH) on LNO surface into lithium polyacrylate (LiPAA) coating layer is demonstrated to facilitate Li$^+$ ion transport. Fine-tuning of the oMWCNT/PAA ratio shows that the electrochemical performance of the LNO cathode is improved when the ionic contribution is increased to 75% of the total coating. Galvanostatic cycling of coated LNO@oMWCNT/PAA (1:3) in a half-cell configuration shows a capacity retention of 92.5% at the end of 100 cycles at 0.2C, while the uncoated cathode retains only 76.7%. In non-optimized LNO//graphite full cells, the capacity retention improves from 68.4 % for the uncoated LNO to 87.5 % for the coated sample. Finally, operando gas evolution analysis of the LNO electrode by OEMS (online electrochemical mass spectrometry) studies shows that the coated electrode produces significantly less amount of gases during the electrochemical cycling, including hindering of oxygen evolution at high voltage compared to the uncoated LNO electrode, proving the positive effect of the oMWCNT/PAA coating.

1. Introduction

In the search for cost-effective cathode materials with high energy density, nickel-containing (Ni>0.6) layered oxides have emerged as the most important candidates for lithium-ion batteries (LIBs) [1–3]. Despite the advantages, their full exploration in automotive batteries is still lagging because increasing the nickel content comes with major challenges. At a Ni content of 80 % and more, there is a strong performance degradation at operating potentials of more than 4.1 V. This is due to intrinsic structural and surface instabilities, which include particle cracking, cation mixing, multiple phase transitions with gas evolution, dissolution of transition metals, etc. [4–7]. In particular, the

cobalt-free LiNiO$_2$ (LNO) as the ultimate Ni-rich cathode suffers from increased chemical surface reactivity due to the strongly oxidizing redox potential of Ni$^{3+/4+}$. However, due to the combination of the triple advantages of relatively low cost, higher specific capacity, and higher voltage, LNO has good reasons to be used for future Li-ion batteries for electric vehicles after the performance issues have been addressed.

Another major drawback that hinders the commercialization of LiNiO$_2$ material is its structural instability at high delithiation states, which leads to a release of oxygen from the lattice with subsequent side reactions with other battery components. The chemical attack of reactive oxygen on organic carbonate-based electrolytes leads to gas formation, internal LIB pressure build-up, and safety issues during cycling

under nominal and abusive conditions. Online electrochemical mass spectrometry (OEMS) is a versatile and powerful technique for investigating gas evolution during lithium-ion battery (LIB) operation[8] providing information on the mechanisms of deleterious side reactions affecting the active materials of the cells that lead to gas evolution, as well as the onset voltages for these phenomena during LIB operation. A deep understanding of the parasitic processes in LIBs is necessary to propose further efficient ways to minimize risks. Despite the exponentially growing number of publications in recent years on the use of OEMS to study LIBs, the effects of surface coatings on the outgassing of cathodes from high-nickel layer oxides have been described only in several publications [9]. Dreyer et al. investigated the impact of trimethylaluminum- and tetraethyl orthosilicate-based coatings on $LiNi_{0.85}$-$Co_{0.10}Mn_{0.05}O_2$, focusing on outgassing during cell cycling between 3.0–4.3 V versus Li/Li^+ using DEMS (differential electrochemical mass spectrometry). They found that the coating reduced the overall CO_2 evolution by more than six times[10]. Liu et al. reported a beneficial effect of surface enrichment with Al on the outgassing of the $LiNi_{0.90}$-$Co_{0.05}Al_{0.05}O_2$ cathode, showing a reduction in CO_2 levels in the enriched sample compared to the standard sample while maintaining 4.4 V hold for six hours, as revealed by OEMS[11]. Surface protection of Ni-rich positive electrode materials has proven effective in reducing or mitigating outgassing at high voltages in solid-state-batteries[12–15].

Among the numerous strategies that have been tried to improve the cathode performance of high-nickel layered oxides, surface modification of the active material particles by applying coatings has gained wide popularity, as most degradation mechanisms are triggered by the surface [16–20]. In practice, a variety of materials such as metal oxides, fluorides, phosphates, conductive polymers, organic compounds, as well as carbon nanomaterials have been explored as coating candidates [17,21]. Nevertheless, no standardized coating material for a Ni-rich cathode has been agreed upon. Although the main purpose of surface protective coatings is to limit the unwanted side reactions of the electrolyte on the surface of the electrode material, they are also required to promote easy Li^+ ion diffusion/electron migration during the charge/discharge processes. However, beyond this assumption, it remains unclear what proportion of each contribution to the coating is optimal to ensure battery performance. There is a lack of in-depth studies on these critical issues, which have a significant impact on the charge transport properties of the active material through the surface coatings.

Our strategy for surface modification of the active LNO cathode material with mixed electron and ion-conducting coatings is pursued to mitigate and understand the degradation mechanisms correlated with the transport behavior of the coatings. The starting LNO material used in this study was procured from BASF which is highly susceptible to contaminations and hence the investigation carried out in this work is a model study focused mainly on studying the impact of coating on Ni-rich cathodes for which commercial LNO was used as a reference material. As a logical approach to improve both types of conductivities, two coating materials are combined, one improving the electronic conductivity and the other increasing the ion mobility. The first goal is surface passivation and the second is to optimize the ratio between electronic and ionic conductivity of the coatings. For the ionic conductive part of the coating, anionic organic polymer polyacrylic acid (PAA) with abundant carboxyl groups is used so that the lithium impurities present on the LNO surface react with PAA to form in-situ LiPAA, which is crucial for Li^+-ion conductivity. In addition, PAA is a non-toxic, inexpensive, and commercially widely available polymer suitable for scaling up. In fact, the precursor PAA or the neutralized LiPAA polymers are widely studied as binders for silicon anodes[22,23] due to the strong interaction capability of carboxylate units with the silanol groups. To a lesser extent, LiPAA as a binder is reported for some high voltage cathodes mainly for aqueous processing[24–29] due to the high electrochemical stability above 4.5 V [23]. For instance, Pieczonka et al., demonstrated LiPAA binder added ex-situ for $LiNi_{0.5}Mn_{1.5}O_4$ (LNMO) spinel high voltage cathode exhibiting improved electrochemical performance despite the

slurry being processed in water compared to the NMP processed PVDF binder [24]. The enhanced performances were attributed to the Li-ion transport properties of LiPAA ($\sim$ 5 mS cm^{-1})[25] and its stabilizing benefit as an artificial cathode electrolyte interface protecting against parasitic side reactions. However, PAA and LiPAA are electronically insulating. It is widely agreed that coatings based on highly conductive carbon nanomaterials can accelerate charge transfer at the cathode surface and create additional electron conduction pathways between active particles and current collectors [26]. In addition, carbon coatings are also able to suppress irreversible side reactions on the cathode surface, which enables an improvement in cycle stability and rate performance. Among the various conductive carbon materials, carboxyl-functionalized multi-walled carbon nanotubes (abbreviated as oMWCNTs in this work) are interesting because they can form an electrically conductive 3D network over the active cathode particles, along with some COOH groups for chemical interaction with metal oxide cathode particles [27,28].

Herein, using different material characterization techniques and electrochemical measurements, we demonstrate the surface stabilization of oMWCNT/PAA-coated LNO with improved capacity retention. More importantly, the study shows that ion diffusion through the coating is a key factor for improved cycling performance rather than electronic transport, as the latter is also enhanced by conductive carbon additives in the electrode composition. In addition, the impact of the oMWCNT/PAA (1:3) coating on the gas evolution of the LNO electrode is investigated using the OEMS technique in galvanostatic and constant voltage ramp electrochemical tests at voltages between 2.5 and 5.0 V vs Li/Li^+. The possible reaction mechanisms are proposed.

2. Results and discussion

2.1. Surface modification of LiNiO₂ and characterization

Fig. 1a shows a schematic representation of the surface modification process of active LNO cathode material with mixed electron/ion conductive coatings. A series of oMWCNT/PAA-coated LNO materials with different ratios of oMWCNT and PAA were prepared by a simple wet coating method using anhydrous ethanol as a solvent. Details of the coating process and acronyms of the samples analyzed in this work are described in the experimental section. For example, the samples LNO@oMWCNT/PAA (1:0) and (0:1) denote coatings consisting only of oMWCNTs or PAA, respectively. As can be seen in Fig. 1a, the mechanism of mixed charge transport through the coating is determined by the combination of in-situ generated Li^+ ion conducting LiPAA and electronically conductive oMWCNTs. It is well known that the surfaces of Ni-rich cathode particles are susceptible to contamination with impurities such as LiOH and Li_2CO_3, which are formed when reacting with H_2O and CO_2 in the air and strongly affect performance [29,30]. Further, the amount of these impurities is found to be proportional to the Ni content in the cathode [31]. Instead of removing the surface contaminations, we have chosen to utilize them advantageously for the in-situ formation of a Li^+ ion conducting LiPAA polymer coating on the LNO surface. However, the Li leaching that occurs during aqueous processing cannot be ignored in Ni-rich cathodes. Therefore, the ex-situ application of LiPAA coating, which inevitably requires water as a solvent, is not very attractive. In this work, LiPAA is to be generated in-situ during the coating process by the reactions of PAA with the remaining lithium species (LiOH, Li_2CO_3) on the LNO surface according to equations (i) & (ii) given in Fig. 1b. To the best of our knowledge, there has been no report on PAA/LiPAA used as a binder or coating for LNO cathode material.

ATR-IR (attenuated total reflectance -infrared) spectroscopy was used to test our design strategy and to identify the presence of coatings with the in-situ generation of LiPAA on the LNO surface. LiPAA was synthesized ex-situ in the laboratory to compare the IR data. From the IR spectra of selected regions shown in Fig. 2a, it can be seen that all coated
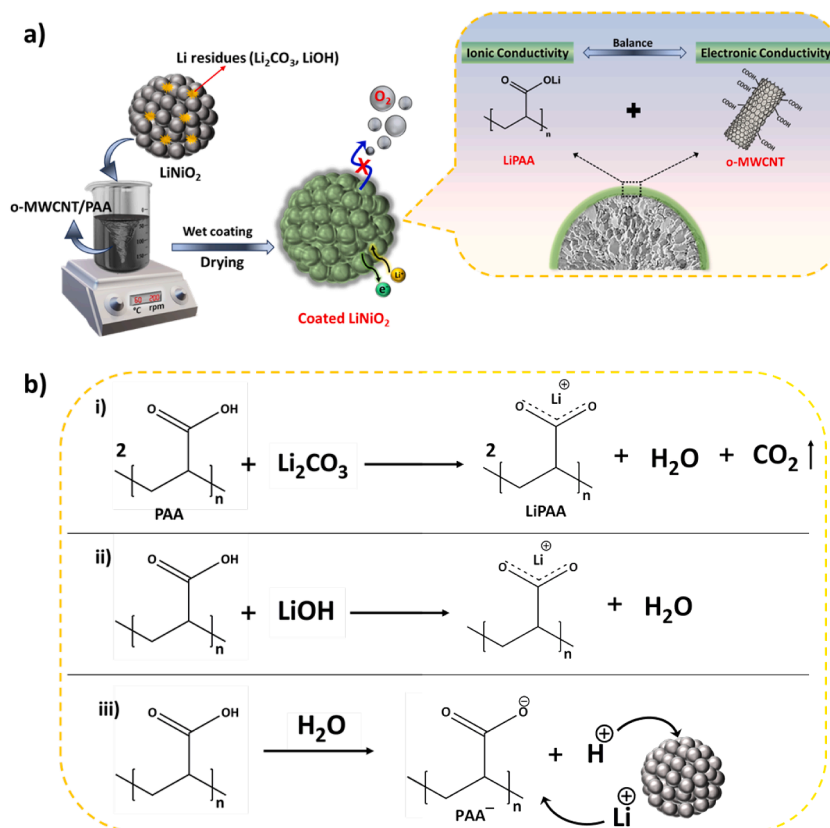
Fig. 1. (a) Schematic illustration of the oMWCNT/PAA mixed conductive coating strategy on LNO particles. **(b)** In-situ reactions of PAA with the residual lithium compounds on the surface of LNO.

LNO samples except LNO@oMWCNT/PAA (1:0) contain a lithium carboxylate peak (-COOLi$^+$ group) at 1557 cm^{-1}, which is consistent with the LiPAA spectra, with peak intensities increasing in proportion to the added PAA content in the coating [30]. At the same time, the absence of the strong PAA peak at 1704 cm^{-1} in these coated samples indicates about 80% conversion of PAA in the coatings to LiPAA. The broad shoulder peak around 1660 cm^{-1}, which collides with the carboxylic $C = O$ bands of the oMWCNTs, makes it difficult to estimate the exact conversion ratio of PAA to LiPAA. Another indication of LiPAA formation in PAA-containing coated samples is the disappearance of the characteristic peak at 870 cm^{-1} attributed to Li$_2$CO$_3$ [31–33]. This particular peak is present in bare LNO as well as in LNO@oMWCNT/-PAA (1:0), where the coating consists only of the carbon nanotubes. Therefore, there is another possible route of in-situ LiPAA formation according to equation (iii) in Fig. 1b, where PAA, which is a weak acid upon deprotonation, can induce lithium leaching from LNO. This deprotonated conjugate base (PAA$^-$) can in turn react with the leached Li$^+$ to form LiPAA and promote the Li$^+$-H^+ exchange reaction. Wood's group recently demonstrated a similar reaction of NMC 811 with PAA as a binder for the preparation of aqueous slurries, in which LiPAA was formed in-situ by the reaction of leached Li$^+$ ions from NMC in water with deprotonated (PAA$^-$), resulting in Li$^+$-H^+ exchange near the cathode surface [27]. However, their study showed that water is very important for this reaction. When ethanol is used as the slurry solvent instead of water, this pathway of in-situ LiPAA formation is not favored, as no lithium carboxylate peaks were observed in the corresponding FTIR spectra. This fact further supports our proposed mechanism of LiPAA formation on the LNO surface, which in this study occurs predominantly via reactions (i) and (ii) with lithium residues, since we use ethanol as the coating solvent. Nevertheless, we believe that it is not possible to completely exclude the chemical delithiation of LNO via pathway (iii), because although no water is used in our coating

formulation, some amounts of water may be formed when PAA reacts with LiOH or Li$_2$CO$_3$. In addition, PAA is known to be a hygroscopic polymer that can also adsorb moisture during storage.

To further verify the presence of a coating and to compare the surface chemistry of the LNO samples, XPS (X-ray photoelectron spectroscopy) measurements were carried out. Fig. 2b shows the full XPS survey spectrum of bare LNO compared to that of LNO@oMWCNT/PAA (1:3), with mainly the four elements Ni, O, C, and Li being detected in both cases, as expected. We selected LNO@oMWCNT/PAA (1:3) for comparison because it showed the best electrochemical performance among the coated samples (see below). The high-resolution C1s spectra for LNO and LNO@oMWCNT/PAA (1:3) are shown in Fig. 2c. Uncoated LNO shows C1s deconvoluted to Li$_2$CO$_3$ species around 289 eV[34] and organic carbon groups at 284.7 eV, which belong to random hydrocarbons[35,36] that are always present in the XPS spectra of Ni-rich cathodes. Firstly, the presence of a significant amount of residual carbonate on the bare LNO shows that it is still a challenge to avoid the formation of carbonate during the calcination phase of the synthesis. In addition, the amount of residual lithium on the surface increases during storage when there is no protective coating [37]. The coated LNO has remarkably lower amounts of Li$_2$CO$_3$ than LNO, which is consistent with our mechanism of LiPAA formation. At the same time, the peak at 287.9 eV, which is negligible in the pure LNO but significant in the coated sample and attributed to the COO group, confirms the presence of LiPAA [38]. The high-resolution O1s spectra (Fig. 2d) show peaks at 529 eV, which can be assigned to the lattice oxygen representing the TM-O bond. The intensity of this TM-O bond decreases in comparison to the $C = O$ peaks (532 eV) in the coated LNO, which means that the proportion of the $C = O$ peak in the coated LNO is higher than in the pure LNO due to the polymers.

The microstructures of the oMWCNT/PAA-coated LNO samples were verified by SEM images. Representative SEM images of the bare and
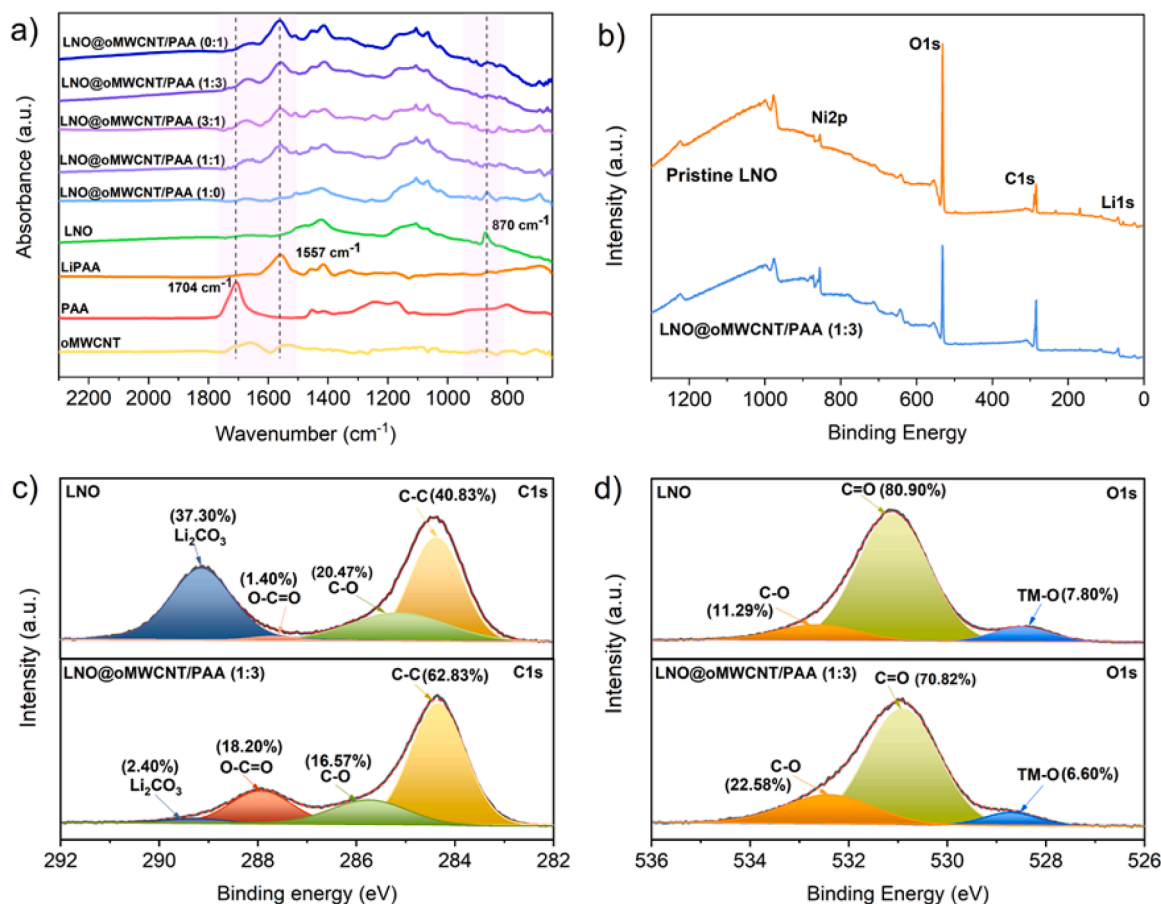
Fig. 2. **(a)** IR spectra of bare LNO compared with oMWCNT/PAA coated samples and starting materials. XPS spectra of **(b)** survey, **(c)** C 1 s, **(d)** O 1 s for LNO and LNO@oMWCNT/PAA (1:3).

LNO@oMWCNT/PAA (1:3) coated secondary particles are shown in Fig. 3 **(a, b) & (c, d)**, respectively. The surface morphology of coated and uncoated LNO differs, as can be seen in the high-magnification images. The uncoated LNO exhibited a clean surface. Compared to the bare sample, the coated sample showed a heterogeneous layer of carbon nanotubes and PAA/LiPAA, in which the LNO particles are sporadically covered with regions of significant coating aggregates as well as random areas of thin surface coverage. Fig. 3 **(e-g)** shows the elemental mapping images of the LNO@oMWCNT/PAA (1:3) sample examined by energy dispersive X-ray (EDX) spectroscopy indicating the homogeneous distribution of Ni, O (from LNO) and C (from oMWCNT/PAA coating). It is evident that the simple wet coating method employed in this study allowed only a modest control over the thickness and conformality of the coating. The SEM images of the other coated samples with different oMWCNT/PAA ratios are given in the supporting information (**Fig. S1**). The actual amount of coating in the samples was determined by TGA (thermogravimetric analysis). From the TGA curves given in **Fig. S2**, expectedly the coated samples exhibit higher weight loss (ca. 3%) than bare LNO, except LNO@oMWCNT/PAA (1:0), which has a slightly lower amount of surface coating (2.15 wt.%).

2.2. Electrochemical performance

To compare the electrochemical performance of the LNO-based cathodes, the cycling behavior of the LNO/Li half cells was first tested in a conventional carbonate-based LP40 electrolyte between 2.8 and 4.3 V. Fig. 4a shows the galvanostatic charge-discharge profiles of the coated and uncoated LNO cathodes at a C/10 rate after the first formation cycle. As can be seen, both the uncoated LNO and all the coated

cathodes except the LNO@oMWCNT/PAA (0:1) sample showed comparable discharge capacities close to 200 mAh/g. The lowest initial discharge capacity of 165.7 mAh/g was delivered by the LNO@oMWCNT/PAA (0:1) sample with the coating consisting solely of an ionic conductive polymer. The trend of capacity loss from the low voltage plateau at 3.5 V is shown in Fig. 4b There is a dependence on the amount of PAA in the coatings, which could lead to lithium leaching and thus irreversible capacity loss. This explains the lower capacity shown by LNO@oMWCNT/PAA (0:1) despite the highest amount of ionically conductive coating. The LNO@oMWCNT/PAA (0:1) sample also shows a weak voltage jump around 3.5 V, indicating that it cannot activate the electrochemical reaction below 3.6 V. At the same time, the charge curves in the same potential range show a slightly increased resistance for LNO@oMWCNT/PAA (0:1), which could be attributed to the thickness-limited diffusion of Li^+ ions through the polymer coating. This is also visible from the comparison of their differential capacity versus voltage graphs (**Fig. S3**), where the first peak in the charge region corresponding to H1 phase transition shifted to higher potentials for LNO@oMWCNT/PAA (0:1), indicating the slow Li^+ transport at the beginning of delithiation. **Fig. S4 (a & b)** presents the first charge-discharge voltage profiles and the corresponding first-cycle Coulombic efficiencies of the cathode samples cycled at 0.1C between 2.8–4.3 V. The difference in capacity decay during the formation cycle highlights the positive impact of the coating on the electrochemical performance of LNO. More importantly, the coated samples—excluding LNO@oMWCNT/PAA (0:1)—showed reduced irreversible capacity losses, resulting in improved Coulombic efficiency compared to uncoated LNO. Studies suggest that large initial capacity losses arise from multiple mechanisms, including sluggish Li^+ re-insertion kinetics during the first
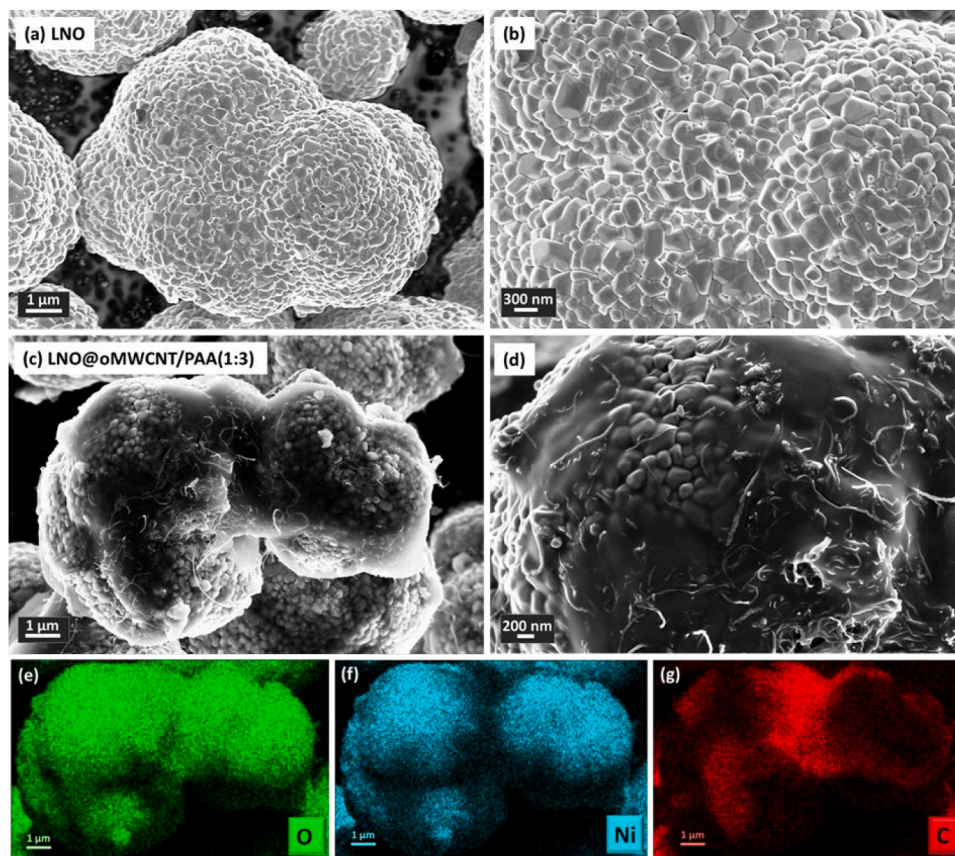
Fig. 3. Low and high magnification FE-SEM images of **(a), (b)** bare and **(c), (d)** oMWCNT/PAA (1:3) coated LNO. Corresponding EDX mapping of coated LNO showing the elemental distribution of oxygen **(e)**, nickel **(f)** and carbon **(g)**.

discharge, loss of active material due to irreversible structural changes, and parasitic electrochemical reactions on the cathode surface[39]. However, since carbonate electrolytes remain electrochemically stable up to 4.3 V, capacity losses between 3.9 V and 4.3 V (vs. Li/Li⁺) are unlikely to be caused by oxidative electrolyte decomposition. This is further supported by gas evolution studies (discussed later). Thus, the primary way in which coatings enhance initial Coulombic efficiency is by preventing irreversible structural changes at the cathode surface that would otherwise occur in the absence of a coating.

Fig. 4c shows the cycling capacity at 0.2C for the bare and coated positive electrodes after the formation cycles at 0.1C for 3 cycles. The capacity of bare LNO cathode drops rapidly from 183.3 to 50.1 mAh/g after 150 cycles, with only 27.3 % capacity retained. In comparison, all surface-modified electrodes exhibited better cycling stability with slower fading rates, which can be attributed to the surface protection provided by the oMWCNT/PAA coatings against side reactions. The cell statistics for the cycling of these cells are given in supporting info **Fig. S5**. The bar graph (Fig. 4d) shows the capacity retention values after 150 cycles together with the discharge capacity values at cycle 1. Of all the coated samples, the half-cell containing LNO@oMWCNT/PAA (1:3) sample with 25 % electronic and 75 % ionic conductivity in the coating showed the best capacity retention of 78.1 % after 150 cycles. **Fig.-S6 (a & b)** shows the corresponding charge-discharge curves at the 1ˢᵗ, 50ᵗʰ, 100ᵗʰ, and 150ᵗʰ cycles for the bare and LNO@oMWCNT/PAA (1:3) electrodes, respectively. However, it should be noted that the cathode with 100 % ionic conductive coating of LNO@oMWCNT/PAA (0:1) also showed a good retention at 76.5 %. A look at the first cycle shows that both controled samples, i.e. LNO@oMWCNT/PAA (1:0) and (0:1) with 100 % either electronic or ionic conductivity component, provided lower initial specific discharge capacity values compared to uncoated LNO, with the former only achieving a capacity retention of 68.5 % after

150 cycles. This observation points to the important fact that both electronic and ionic conductivity are critical for optimal charge transport through the surface coatings, while enhancing only one type of conductivity does not result in better performance. For the remaining three coated samples with different oMWCNT/PAA ratios, the initial discharge capacities are closer to the uncoated ones, with only 1–3% difference. However, the capacity retention and cycling stability are better for the LNO@oMWCNT/PAA (1:3) than for the (1:1) and (3:1) coated electrodes. Therefore, due to the combination of best cycling stability, capacity retention, and optimal specific capacity values, LNO@oMWCNT/PAA (1:3) represents the balanced ratio of electronic and ionic conductivity desirable for protective surface coatings for high-performing LNO cathodes. This specific ratio of 1:3 between electronic and ionic conductivity indicates that the electrochemical reaction rate is mostly limited by Li⁺ ion transport rather than by electron transport.

Taking into account the optimal performance of the LNO@oMWCNT/PAA (1:3) with a balanced electronic/ionic conductive oMWCNT/PAA coating ratio, this electrode was selected for further rigorous electrochemical performance analyses. Due to the high reactivity of Li metal with conventional carbonate electrolytes, the LP40 electrolyte was replaced with a concentrated ether electrolyte containing lithium bis(fluorosulfonyl)imide in 1,2-dimethoxyethane at a molar ratio of 1:4 (LiFSI-4DME) ether electrolyte, which can effectively stabilize the metal anode [40,41]. Fig. 5a shows the comparison of cycling performance of LNO and LNO@oMWCNT/PAA (1:3) half cells with Li metal anode at 0.2C using LiFSI-4DME electrolyte at room temperature. In general, better cycling stability is observed, even for the uncoated cathode using the LiFSI-DME electrolyte compared to LP40. However, the initial discharge capacity of LNO@oMWCNT/PAA (1:3) is also about 10 % lower than that of bare LNO. Nevertheless, the coated LNO shows uniform cycling stability with a capacity retention of 92.5 % after 100
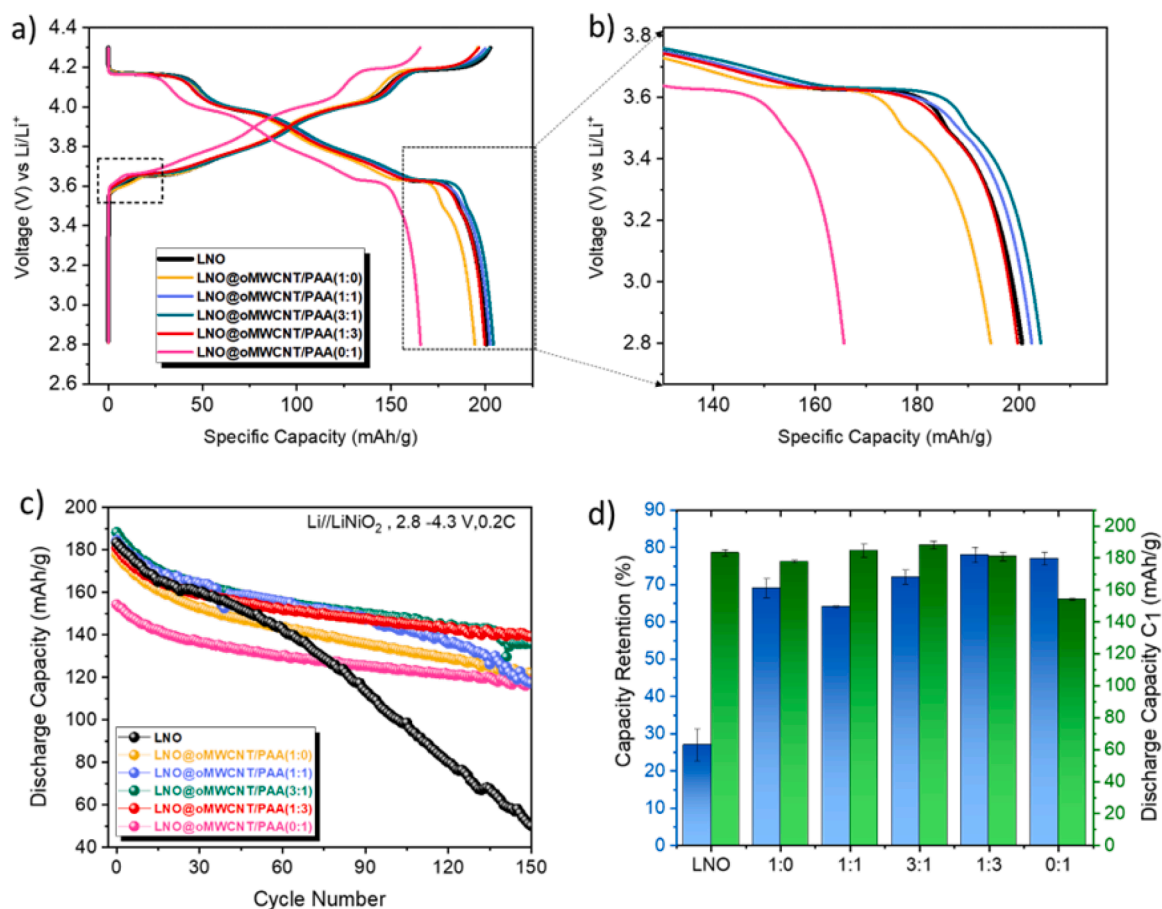
Fig. 4. **(a)** Initial voltage profiles of bare and coated LNO cathodes vs Li metal anode in half cells cycled at 0.1C after the first formation cycle in LP40 electrolyte and **(b)** magnification of the corresponding low voltage plateau region. **(c)** Cycling performance of the same cells at 0.2C rate and **(d)** bar graph showing the trends for discharge capacities at the first cycle and their retention after 150 cycles (error bars: standard deviation of two cells each for each sample).

cycles, while the uncoated sample retains only 76.7 % of its initial capacity, demonstrating fluctuating coulombic efficiency. Fig. 5b shows the corresponding voltage profiles of the first and 100th cycles for LNO and LNO@oMWCNT/PAA (1:3) half cells. Comparing the voltage plateau near 4.1 V, the voltage drop in the 100th cycle is higher for the uncoated LNO than for the coated one, which is due to the increased loss of active lithium and related overvoltage [42,43]. The lower polarization at the end of 100 cycles for the LNO@oMWCNT/PAA (1:3) indicates a limited structural degradation achieved via the optimized surface protection.

The long-term cycling performance of the LNO-based electrodes was investigated in half cells at a rate of 1C, as shown in Fig. 5c. Before the long-term cycling, three activation cycles were performed at 0.1C. The charge-discharge profiles corresponding to the first two formation cycles are shown in **Fig. S7**. The first charge curve of the formation cycle for the coated and uncoated samples appears at a higher voltage compared to the subsequent cycle, indicating a higher initial resistance. For the uncoated Ni-rich cathodes, this feature can be attributed to the residual insulating lithium-containing layer, which disappears in the next cycle due to decomposition during the first charge [44]. However, in the case of the coated sample, this voltage increase can be attributed to the additional resistance provided by the coating layer over the residual impurity layer. Fig. 5c shows that the specific discharge capacities of both samples decrease at high C rates. The initial discharge capacity of LNO@oMWCNT/PAA (1:3) is about 20% lower than that of uncoated LNO at 1C, Fig. 5c. The uncoated LNO exhibited an initial specific discharge capacity of 183 mAh/g, of which only 69.4% was retained at the end of 200 cycles. In contrast, the coated LNO showed excellent

capacity retention of 95.2% under the same cycling conditions. The poor cycling performance of the uncoated LNO at high C-rate due to increased surface reactivity demonstrates the importance of protection by the oMWCNT/PAA coating. In addition, the voltage-capacity curves at 1C corresponding to the 1st, 50th and 100th cycles for the unprotected and the LNO@oMWCNT/PAA (1:3) half cells (**Fig. S8 (a & b)**) show that the average voltage of working plateau for the uncoated cathode decreases rapidly with increasing number of cycles, while the coated cathode keeps the high voltage constant during long-term cycling. This means that the presence of the coating helps to preserve the structure of the Ni-rich positive electrode over long-term cycling. The rate performance investigations of half cells with uncoated LNO and LNO@oMWCNT/-PAA (1:3) cathodes at varying current rates from 0.1C to 5C were tested in the LiFSI-4DME electrolyte (**Fig. S9 (a)**. The cells were cycled at each rate for 5 cycles. The rate capabilities of both the cells with uncoated and coated electrodes exhibit a very similar behaviour, except that at the beginning of the cycle at C-rates up to 1C, the LNO@oMWCNT/PAA (1:3) shows lower discharge capacities than the uncoated cathode, which is similar to their long-term performance test. However, from the capacity retention graph (**Fig. S9 (b)**) it is evident that coated LNO outperforms the uncoated one at all C-rates. This suggests that even though there is an initial sluggish kinetics of lithium diffusion through the coated material, after a certain number of cycles, a stable interface is established, which enables better cyclability even at higher C-rates. Although the exact reason for the lower initial specific discharge capacity of the coated LNO is not clear, we believe that this is primarily due to the fact that as the salt concentration increases such as in LiFSI-4DME, the viscosity of the electrolyte increases and thus the
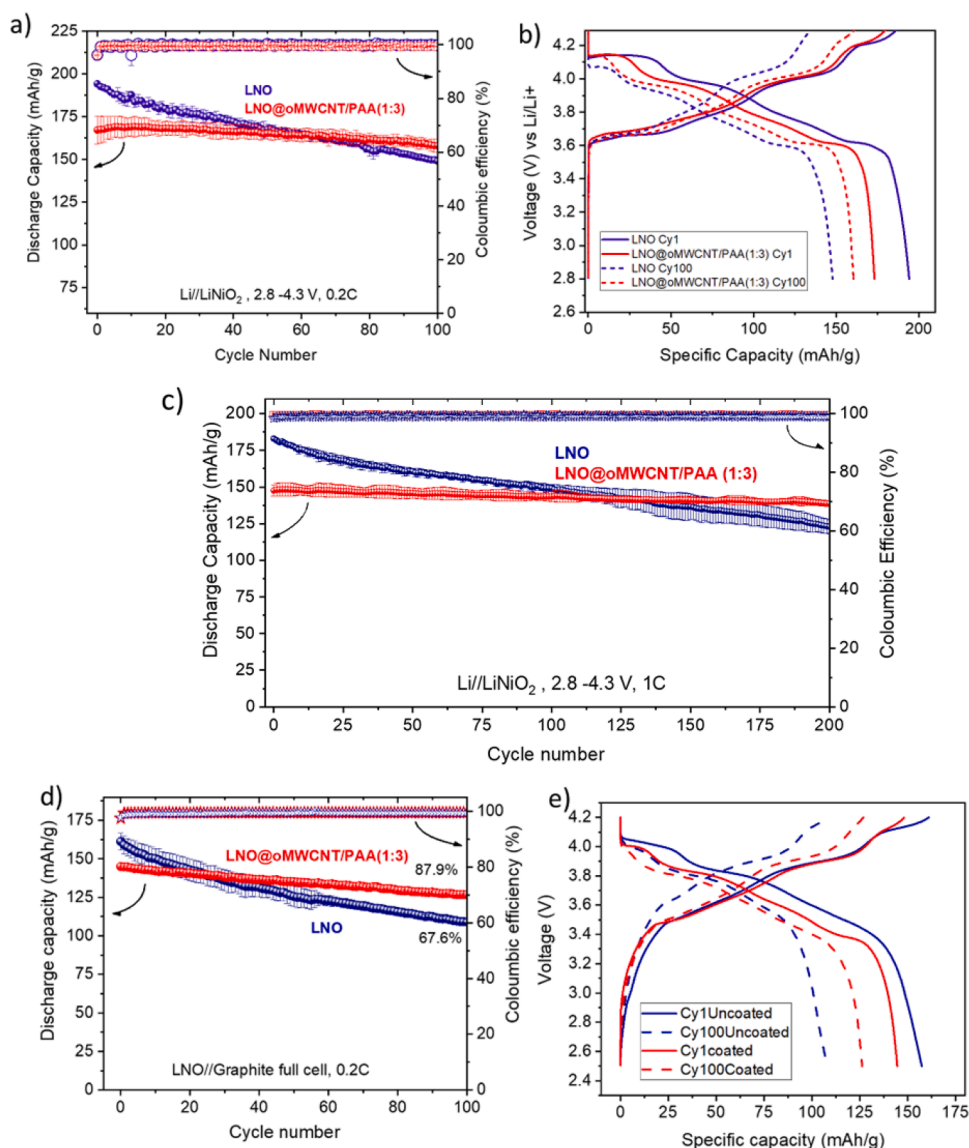
Fig. 5. **(a)** Cycling performance of uncoated and coated LNO-based half cells in the potential window 2.8 −4.3 V using LiFSI-4DME electrolyte at 0.2C and **(b)** their corresponding voltage profiles for the 1st and 100th cycle. **(c)** Long-term cycling performance of the cells at 1C rate. **(d)** Full cell cycling performance of coated and uncoated LNO versus graphite anode in LiFSI-4DME electrolyte at 0.2C rate and **(e)** their corresponding charge-discharge profiles for the 1st and 100th cycles (error bars: standard deviation of two cells each).

wettability decreases, which also contributes to the lower initial capacity. In addition, this wettability problem is accelerated in the presence of coatings initially.

The performance improvement of the coated compared to the uncoated LNO materials becomes even more evident in a full cell configuration using a graphite anode. Fig. 5 **(d & e)** compares the performance of the full cells in LiFSI-4DME electrolyte at 0.2C and the corresponding voltage profiles for the first and 100th cycles. It was found that the capacity retention of the LNO//graphite full-cells improves from 68.4% for the uncoated LNO to 87.5% for the sample coated with LNO@oMWCNT-COOH/PAA (1:3), yet the initial discharge capacities are lower for the coated LNO. A lower capacities in the full cell with graphite electrode originate in irreversible losses occurring on the graphite electrode.

2.3. Postmortem analysis

To investigate the effect of the oMWCNT/PAA coating acting as a protective interface providing structural stability to the electrodes to withstand long term cycling and suppress gas evolution behaviour,

electrochemically aged electrodes were firstly analyzed by SEM. Generally, there are two types of cracks occurring in the case of Ni-rich cathodes – (i) intra-grannular cracks initiated from the inside of the structure and (ii) intergranular fracture, also known as the grain boundary fracture, which occurs due to the anisotropic volume change of the primary particles. In the case of surface-protected active materials, it is primarily aimed to overcome the inter-granular cracking rather than the intra-granular. For this purpose, upon analyzing the surface morphology after cycling, in this study, we found that oMWCNT/PAA coating is able to significantly reduce the surface cracking of the active materials compared to the uncoated LNO (Figs. **S10 and S11**). More importantly, it is noted that even though there are some surface cracks unavoidably formed, the oMWCNT/PAA coating is found to prevent the severe shattering of the particles (seen in the case of uncoated LNO) by holding them together throughout the cycling (**Fig. S12**). Additionally, to understand the influence of this coating on the intragranular cracking in correlation with the gas evolution behaviour known for the Ni-rich cathodes like LNO, cross-sectional FIB-SEM analysis was also conducted. For comparison, the

cross sections of coated and uncoated LNO cathodes before cycling were measured (**Fig. S13**), which showed no internal cracking as expected. Interestingly, in the case of cathodes after cycling, the study showed that with the protective oMWCNT/PAA coating even the intragranular cracking was significantly mitigated in comparison to the uncoated LNO as evident from the high magnification SEM images given in **Fig. 6(a) and (b).** Additional low and high magnification images of the cycled coated and uncoated cathodes are given in **Fig. S14** from which it is evident that uncoated LNO suffers from severe structure destruction due to intra-granular cracking. The oMWCNT/PAA coated LNO, on the other hand, undergoes very milder internal fractures but no extreme structure destruction. Nevertheless, it was also noted that oMWCNT/PAA was sporadically covered with average thickness varying around 250–300 nm (**Fig. S15**).

Further, in order to get a closer insight into the structural changes at the interface between LNO and coating, atomic resolution TEM imaging was performed. **Fig. S16** depicts various magnifications of the thinned pristine and cycled secondary LNO particles, surrounded by a coating of varying thicknesses. At higher magnification, the pristine coated particle demonstrates a rather undisturbed bulk layered structure. In the bulk, pristine LNO retains a layered structure with (R-3 m), while its surface termination layer exhibits contrast variations consistent with the presence of Li/Ni cation disorder in the last 2–5 nm (Fig. 6(c)). Overlaying MWCNT/LIPAA coating remains structurally distinct. Electrochemical cycling induces surface reconstruction due to the O loss, triggering collapse of the layered (R-3 m) bulk into a cation-disordered rocksalt phase (Fm-3 m) at the surface due to Ni^{2+} migration into Li layers (Fig. 6d). Upon cycling, this disordered region has a thickness of 10–14 nm. Above the degraded surface, the MWCNT network remains evident, emphasizing the protective nature of the coating.

2.4. OEMS investigation of LNO electrodes based on bare and coated active materials

The OEMS method was applied to understand the impact of oMWCNT/PAA (1:3) coating on the outgassing of LiNiO$_2$ electrodes at different cut-off voltages. The configuration of the cell was chosen to avoid the possible contribution of the negative electrode to gas formation during cycling. For this purpose, an electrochemically delithiated LiFePO$_4$ (LFP) counter electrode with a customized loading was used during the OEMS test. During the electrochemical testing of LNO / delithiated LFP (FP) cells, none of the electrodes are exposed to low voltages, which avoids the formation of SEI layer on the negative electrode and the associated gas evolution. In addition, the LFP electrode
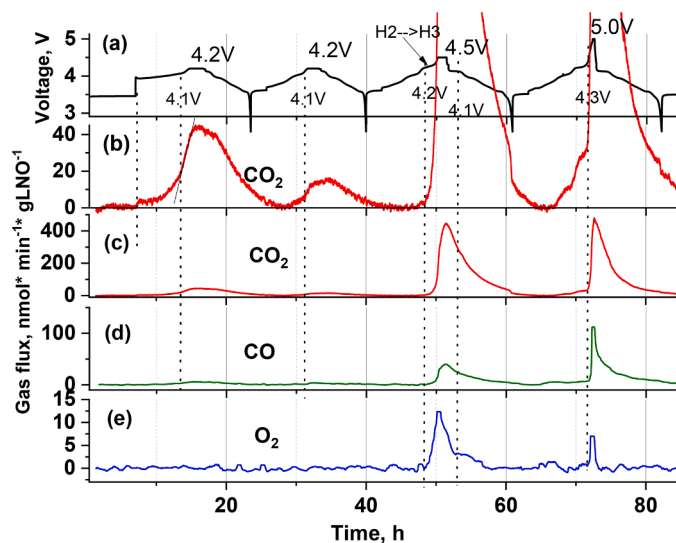

Fig. 7. Voltage vs time profile for the cell containing LiNiO$_2$ bare positive electrode, FP negative electrode, and EC/1.3 M LiPF$_6$ electrolyte cycled at different upper cut-off voltages at C/10 (a); associated molar fluxes of CO$_2$ (b, c), CO (d) and O$_2$ (e).
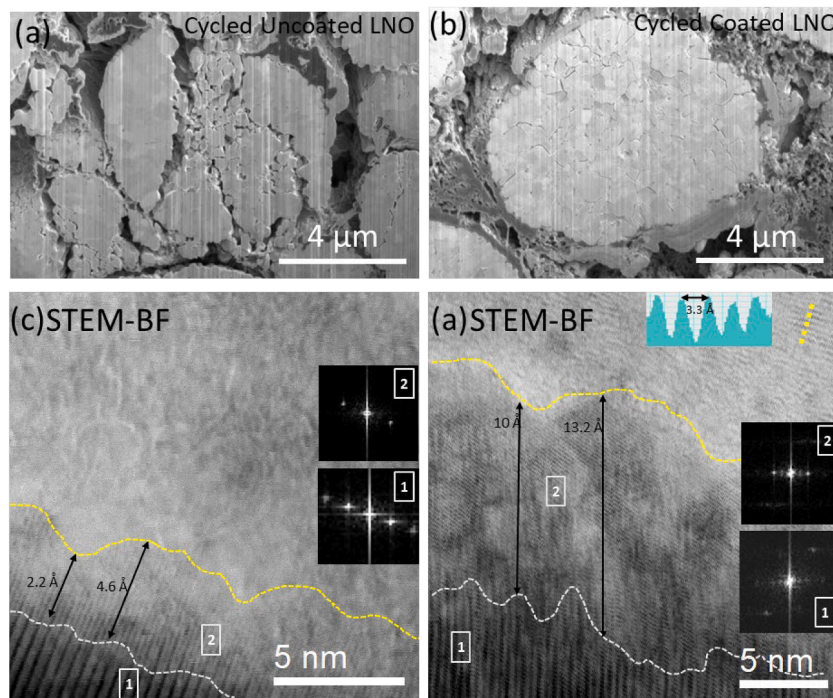

Fig. 6. FIB-SEM cross-section images of uncoated LNO **(a)** and coated LNO@oMWCNT/PAA **(b)** electrodes after long term cycling in half cells in the potential window 2.8 −4.3 V using LP40 electrolyte at 0.2C. STEM-BF images of **(c)** pristine and **(d)** cycled (150 cycles) LNO@oMWCNT/PAA LNO cathodes. Yellow and white dashed lines show the boundaries between layered bulk and disordered surface structure (white) as well as between disordered surface structure and coating (yellow). The inset in b) represents the intensity profile (short yellow dashed line) over the carbon nanotube stemming from the coating.

does not generate any gas during the cycle itself.

Fig. 7 and Fig. 8 show voltage vs time profiles for the LNO/FP cells during 4 cycles with upper cut-off limits of 4.2 V (2 cycles), 4.5 V, and 5.0 V vs Li/Li$^+$ along with the corresponding flux of gases for the cells with bare and coated LNO electrodes, respectively. The voltage and specific capacity curves for these cells are shown in **Figs. S17 and S18**. The typical cycling limit of 4.2 V was taken to probe the gas formation under nominal electrochemical conditions, while the OEMS analysis at elevated voltages of 4.5 V and 5.0 V could provide insight into the protective function of the coating under abusive conditions and thus giving access to the safety characteristics. Three typical gases were observed during the OEMS experiment, with the main contribution of CO_2 and lesser amounts of CO and O_2 in Fig. 7 and Fig. 8, consistent with literature data [9]. The first cycle is characterized by relatively high emissions of CO_2 and CO. This is due to the oxidation of residual lithium carbonate on the surface of the LNO electrode [45]. The shapes of the CO_2 evolution profiles are different for bare and coated LNO electrodes, implying that the coating affects CO_2 formation during the first charge. This can be related to the fact that some amount of Li_2CO_3 was consumed by the reaction with PAA for the coated LNO electrode, as discussed above, see Fig. 2a. In addition, the maximum CO_2 flux achieved is higher for the bare electrode. The highest CO_2 and CO fluxes are observed at 4.2 V for the first two cycles, which is probably related to a slight evolution of reactive oxygen (not detected by OEMS) at the end of the charge, followed by chemical oxidation of the electrolyte [46]. The second cycle with a cut-off of 4.2 V shows a modest CO_2 / CO evolution with no significant differences between the bare and coated LNO electrodes. It should be mentioned that the specific capacities obtained during the cycle up to 4.2 V were 20–40% lower for the coated LNO electrode than for the uncoated LNO (**Figs. S17 and S18**). Therefore, a difference in delithiation states could contribute to the lower outgassing of the coated LNO electrode under these conditions.

Significant gas formation for both investigated electrodes was observed during the third cycle with a cut-off limit of 4.5 V vs Li/Li$^+$ in Fig. 7 and Fig. 8. Under this condition, a complete conversion of the H2 phase to H3 takes place in LNO [47]. The instability of the H3 phase leads to the release of reactive oxygen ($^1O_2$) through the LNO lattice, which is accompanied by the oxidation of the electrolyte and the outgassing of LIB. Fig. 7 and Fig. 8 show the beginning of the release of all gases, including oxygen, at about 4.2 V with a maximum of 4.5 V,
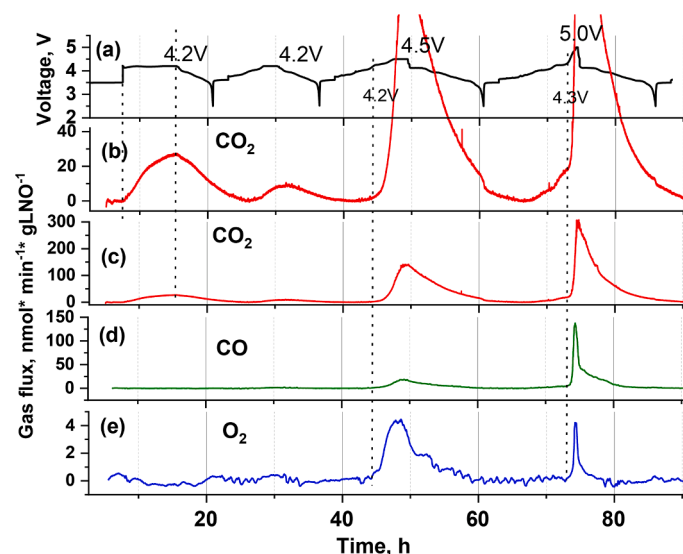
followed by a decrease in gas fluxes at the beginning of the third discharge. Chemical oxidation of the ethylene carbonate-based electrolyte is a dominant mechanism for the formation of CO_2 and CO during the third cycle. The shoulder visible for the oxygen evolution curve at about 4.1 V during a discharge in Fig. 7(e) and Fig. 8(e) probably corresponds to the structural rearrangement of LNO and is consistent with the results reported by Biasi et al. [47].

The fourth cycle represents abusive cell test conditions with an upper cut-off limit of 5.0 V held for 15 min. In this case, the onset point of CO_2 evolution shifts to 4.3 V vs Li/Li$^+$ in Fig. 7 and Fig. 8, but smaller CO_2 spikes still occur at lower voltages, similar to the previous cycles. The amount of O_2 released is lower compared to the 3rd cycle. Most of the reactive oxygen was likely evolved from the LNO lattice during the 3rd cycle, leaving only a small amount for the next cycle. Regarding the mechanism of CO_2 and CO production, chemical oxidation of the electrolyte by reactive oxygen and direct electrochemical oxidation of organic carbonates at voltages >4.7 V versus Li/Li$^+$ are the most important factors, with some contribution from electrooxidation of carbon black [48].

As can be seen from Fig. 7 and Fig. 8, the main characteristics and starting points of gas evolution are similar for the bare and coated LNO electrodes. However, there is a significant difference in terms of the
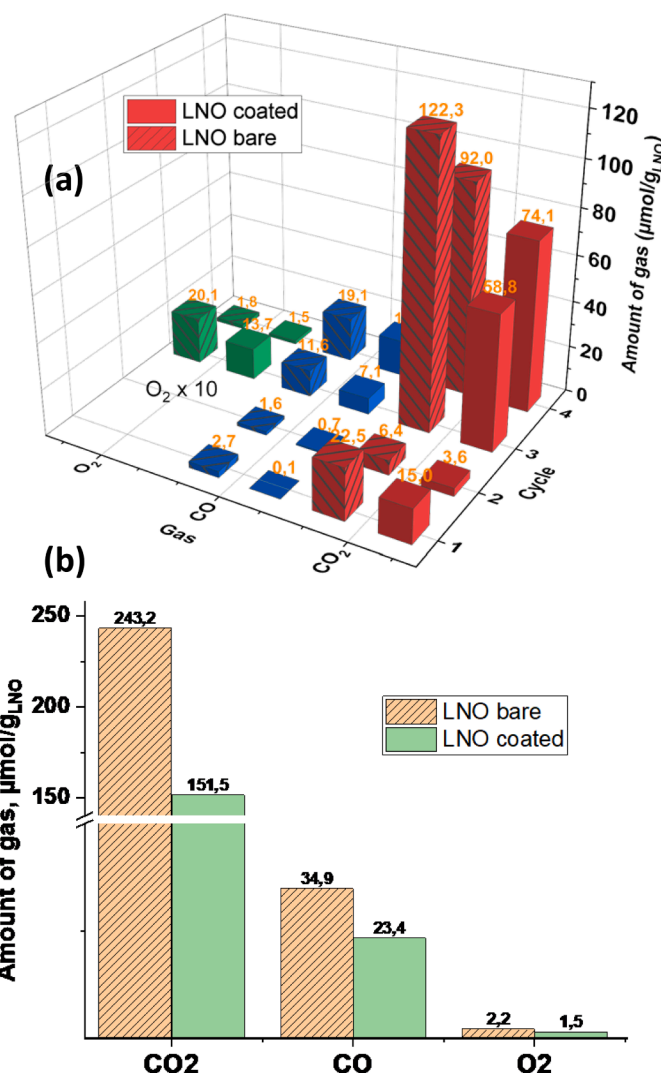
Fig. 9. Amounts of CO_2, CO, and O_2 generated during the cycles 1–4 by the LNO electrodes, the amounts of O_2 are multiplied by 10 for better presentation (a); total amounts of gases obtained during 4 cycles for bare and coated LNO electrodes (b).

Fig. 8. Voltage vs time profile for the cell containing $LiNiO_2$ positive electrode coated with oMWCNT/PAA (1:3), FP negative electrode, and EC/1.3 M $LiPF_6$ electrolyte cycled at different upper cut-off voltages at C/10 (a); associated molar fluxes of CO_2 (b,c), CO (d) and O_2 (e).

outgassing rates and the amount of gases evolved. Fig. 9 shows the gas quantification results for each cycle during the OEMS experiment with bare and coated LNO electrodes. In all cases, the coated LNO electrode produced 1.5–2 times less gases than the uncoated electrode. This result is significant and was confirmed by a reproducibility study. The most remarkable difference was observed during the 3rd cycle, where the largest release of reactive oxygen took place. This means that the coating on the surface of the LNO particles can limit the harmful effects of reactive oxygen on gas formation in LIB at high voltage. The mechanism behind this may be either a mechanical covering of the surface of the LNO particles with oMWCNT/PAA, preventing their direct contact with the electrolyte, or a partial neutralization of the released oxygen by gas-free reactions involving the coating. This point requires further investigation and will be the subject of our future work. It should be mentioned that the specific capacities obtained in the 3rd and 4th cycles for the bare and coated LNO electrodes in **Figs. S17** and **S18** were very close to each other with ~5% difference. This means that similar LNO delithiation states were compared during the 3rd and 4th cycles in the present study and that the coating did not affect the electrochemical performance of the electrode, at least at low C rates.

The impact of the o-MWCNT/PAA coating on gas generation by a LIB was further investigated using cyclic voltammetry. It was interesting to compare the effects of the coating on the outgassing of the cell under different electrochemical conditions. **Fig. S19** shows the cyclic voltammograms obtained for bare and coated LNO working electrodes versus FP at a very slow scan rate of 3 mV/min. It is noticeable that the direct scan for bare and coated electrodes shows many differences. The onset of the current rise is positively shifted by about 400 mV for the electrode with oMWCNT/PAA, which means an increased resistance for this active material, probably due to the coating. However, the back scan is similar for both electrodes and contains typical features for the LNO electrode [49]. Associated gas formation is compared in **Fig. S20** for the bare and coated LNO electrodes. Similar to the OEMS experiment with galvanostatic cycling in Fig. 7 and Fig. 8, CO_2, CO, and O_2 were observed, with the main contribution coming from CO_2. The starting points for CO_2 and O_2 evolution in both cases are 4.0 V and 4.4 V, respectively. **Fig. S20** shows that some of the maxima on the CO_2 and CO evolution profiles for both electrodes are closely related to the highest O_2 formation rates. This is indeed evidence of an important contribution of chemical electrolyte oxidation to the overall gas formation, in agreement with the literature[46]. The most remarkable feature is the shape of the O_2 evolution curve in **Fig. S20 (a,b)**. It can be seen that while the bare LNO exhibits a rather high O_2 flux right after the starting point, this process is hindered in the case of the coated active LNO material, leading to a moderate, gradual increase in O_2 flux up to 4.8 V. The total amounts of gases generated during the CV cycles are shown in **Fig. S21**. Comparing the data with Fig. 9, the main trends confirm the above results – reduced amounts of all gases evolved by the oMWCNT/PAA coated electrode. The ratios for CO_2 and CO amounts between bare and coated LNO are within 1.3–1.6, but the difference is greater for O_2 formation during the CV experiment: the bare LNO electrode evolved 4 times more O_2 than the coated electrode. In principle, the LNO electrode is exposed to high voltages (>4.5 V) for a much longer time compared to galvanostatic cycling (~5 h versus ~1 h), that is why higher absolute amounts of gas were obtained. It appears that oMWCNT/PAA was particularly efficient in limiting the outgassing of LNO at high voltages despite the longer exposure time. This confirms a positive influence of the oMWCNT/PAA coating on the suppression of gas formation by LIB under extreme conditions with an organic carbonate-based electrolyte observed under constant current and constant voltage ramp electrochemical conditions.

3. Conclusions

To summarize, a facile mixed electron/ion conductive protective coating on LiNiO$_2$ cathode materials (LNO) was demonstrated based on

oMWCNT and PAA. In particular, the PAA coating was beneficial in reducing the lithium residues (LiOH/Li$_2$CO$_3$) on the cathode surface by converting them into Li$^+$ ion conducting LiPAA layers as revealed by the IR and XPS analysis. The robust optimized oMWCNT/PAA coating on LNO proved to establish a stable interface by minimizing the parasitic interactions between the cathode and electrolyte, indicated by the enhanced electrochemical performance of the coated electrode in half and full cell configurations. Discharge capacity retention for the full cells containing oMWCNT/PAA-coated LiNiO$_2$ vs graphite increased by 19% after 100 cycles at 0.2C compared to the cells with an unprotected positive electrode. It is also shown that the coating significantly limits the structural collapse for LiNiO$_2$ active material, as evidenced by a drop in average voltage during cycling. Most critically, the performance improves when the ionic contribution of the coating increases to $\geq$ 75%. The study shows that Li$^+$ ion diffusivity is the limiting factor and not electron transport. Although both are required, the ratio between electronic and ionic conductivity components should be about 1:3. The results are very promising from a practical point of view, as the oMWCNT and PAA coating materials used are commercially available nanomaterials that can be easily integrated into the scale-up processes.

The outgassing of bare and coated LNO electrodes was compared using the OEMS technique to demonstrate the effects of oMWCNT/PAA coating on gas production and potential safety issues at upper cycling cut-off voltages between 4.2 and 5.0 V. It was found that CO_2 is the main gas formed during the electrochemical reactions, with some contributions from CO and O_2. In general, the coating reduced the amount of gases produced by the LNO electrode in the galvanostatic and cyclic voltammetry electrochemical test modes. CO_2 production was reduced by a factor of 2 up to 4.5 V and by a factor of 1.2 – up to 5.0 V at constant current, assuming similar specific capacities for both electrodes under the given electrochemical conditions. The significantly lower CO_2 evolution observed from the coated LNO is attributed to the consumption of detrimental Li$_2$CO$_3$ by PAA coating during the in-situ generation of LiPAA. The coated LNO electrode released 1.5 times less O_2 in a galvanostatic test and 4 times less O_2 in a cyclic voltammetry test. In addition, it was found that the kinetics of oxygen evolution was hindered in the coated electrode during a cyclic voltammetry experiment between 4.4 V and 4.8 V. This result is consistent with the improved structural stability of the coated LNO active material that was observed during long-term cycling. It can be concluded that the application of oMWCNT/PAA coating on the surface of LiNiO$_2$ particles is a promising way to reduce the excessive gas generation by the cathode material and improve the safety of high energy density LIBs. This work contributes to the practical application of the active LiNiO$_2$ material in real-life LIBs.

4. Experimental section

Materials: LNO powder was obtained from BASF and stored in an Argon-filled glovebox kept with H$_2$O and O$_2$ levels below 1 ppm. Multi-walled carbon nanotubes (MWCNTs) (Nano Tech Labs, 12,111 C-grade) and poly (acrylic acid) (PAA) (Sigma Aldrich, Mw= 450,000) were used as received. All the solvents and reagents used were high-purity grade purchased from Sigma Aldrich. The materials for battery fabrication were obtained from commercial sources which include Li metal foil (thick non-FMC-110 μm), Celgard™ 2320 separator (Celgard Co.), LP40 commercial electrolyte (1 M LiPF6 in EC: DEC 1:1 (v:v) Elyte innovations), Lithium bis(fluorosulfonyl)imide (LiFSI) salt (99.0%, Solvionic), 1,2-Dimethoxyethane (DME) solvent (HPLC grade 99.9%, Sigma Aldrich), Polyvinylidene fluoride binder(PVDF) (Sigma Aldrich) and Super C65 carbon black (Timcal). The concentrated LiFSI-4DME electrolyte was prepared by mixing the LiFSI salt and purified DME solvent in a specific LiFSI: DME molar ratio 1:4. Prior to electrolyte preparation, the DME solvent was dried over 4 Å molecular sieves for 5 days followed by refluxing with Na/K alloy overnight and then purified by fractional distillation. The solvent drying as well as electrolyte preparation steps were carried out inside argon-filled glove box.

Synthesis of surface-modified LiNiO$_2$ (LNO): The obtained LNO active materials were coated with mixtures of mildly oxidized multi-walled carbon nanotubes (oMWCNT) and polyacrylic acid (PAA) in a one-step process using the wet coating method. In brief, calculated amounts of oMWCNT and PAA were dispersed in anhydrous ethanol by ultrasonic treatment, followed by the addition of LNO powder, and the mixture was continuously stirred at 60 °C. After evaporating the solvent, the residue was dried in a vacuum oven at 110 °C overnight. A series of coated LNO samples were prepared by varying the amounts of oMWCNT and PAA between 100 - 0 % while maintaining the total coating content to 3 wt.%. Table 1 shows the abbreviations of the o-MWCNT/PAA-coated LNO samples with different composition ratios of the coating components investigated in this study. The lithiated LiPAA used as a reference for the FTIR comparison was synthesized in the laboratory by the neutralization reaction of equimolar amounts of PAA and LiOH in water.

Characterization: Infrared (IR) spectra of powder samples were recorded using an ATR-IR (attenuated total reflectance-infrared) Alpha II (Bruker) instrument equipped with germanium crystal. Each measurement was collected and averaged over 48 scans in the 4000 - 400 cm^{-1} range. Thermogravimetric analysis (TGA) was performed under argon flow, in the temperature range between 35 °C and 1000 °C using TGA Q5000 (TA instruments) at a heating rate of 10 °C min^{-1}. Morphology and elemental mapping of the samples were carried out using a Supra 35 Carl Zeiss FE-SEM (field emission-scanning electron microscope) equipped with an Ultim Max 100 EDX (Energy Dispersive X-ray spectroscopy) detector. The accelerating voltage was set to 10 kV for SEM/EDX. XPS (X-ray photoelectron Spectroscopy) measurements were performed using a PHI Versaprobe 3AD system (Physical Electronics). The X-ray excitation source used was Al-Kα1 (1486.6 eV) radiation. Ion and electron beam charge neutralization were applied to all acquisitions on 200 μm sample spot size. Fitting of the XPS spectra was performed using PHI Multipak software with Shirley background correction and Gaussian-Lorentzian curves. Shift correction of the spectra was done by aligning the C1s peak to 284.8 eV.

FIB cross-sectional analysis and TEM lamella preparation were performed by using a FIB-SEM Helios G5 UC equipped with a Multi gas injection system (GIS), a CleanConnect sample transfer system, and an Easy Lift nanomanipulator for TEM sample lift-out (Thermo Fisher Scientific, The Netherlands). Samples and FIB lift-out grid were mounted into a CleanConnect capsule inside Ar Ar-filled glovebox and transferred in Ar 5.0 overpressure (200 mbar) directly to the FIB instrument. The sample surface was initially protected by 400 nm W layer by using electron beam induced deposition (EBID, 2 kV @ 0.8 nA). Subsequently additional, W layer was deposited by using Ga+ ion beam induced deposition (IBID, 30 kV @ 0.43 nA) to achieve a protective layer with a final thickness of 1,7 μm. The cross section was performed with focused Ga+ ions at 30 kV @ 21 nA, with the FIB currents reduced stepwise to 0.8 nA for the final ion polishing step. Morphological images of the cross sections were recorded using a low-energy electron beam (2 kV @ 50 pA) by using a standard ETD and ICE detector.

A rough lamella chunk with dimensions of 20 × 8 μm was milled, thinned to 2 μm and transferred to an FIB grid using an Easy Lift nanomanipulator. Due to sample sensitivity, lamella was first thinned to 250 μm thickness using FIB at 30 kV by sequentially reducing ion beam

currents from 790 pA to 80 pA. Subsequently, lamella was carefully thinned to 100 nm using FIB at 16 kV with 20 pA beam current. Afterwards, lamella was sequentially polished on both sides using FIB at 5kV@50 pA and 2kV@25 pA until electron transparency (~60 nm). As prepared lamella sample was transferred with CleanConnect capsule back to glovebox, where it was mounted to the TEM vacuum transfer holder. They were cut out of pristine and cycled cathodes and transported in an air-tight carrier (CleanConnect, ThermoFisher Scientific) into the argon-filled glove box. There, the samples were transferred onto the vacuum transfer TEM holder (Gatan, USA) one at a time. TEM work was performed on JEM ARM200CF analytical TEM (JEOL, Japan) equipped with probe Cs corrector and cold FEG.

Cell assembly and electrochemical measurements: All electrochemical tests were carried out in pouch-type battery cells using a VMP3 Bio Logic VMP3 potentiostat at room temperature. The cells were assembled inside an Ar-filled glove box with oxygen and water levels maintained below 1 ppm. The homemade pouch cell consisted of a triplex foil (PE 90 μm /Al 10 μm/ PET 20 μm) inserted with 3 mm wide Al and Cu foil strips for cathode and anode contacts, respectively. For the fabrication of cathode working electrodes, either uncoated or coated LNO powder, Super C65 carbon black, and PVDF in the mass ratio 92.5: 4:3.5 were dispersed in NMP. This mixture was subjected to 1-hour SPEX milling until a homogeneous slurry was obtained. The slurry was then cast on carbon-coated aluminium foil by standard doctor blade technique and dried at 80 °C for 2 h in air. Subsequently, 16 mm cathode discs were punched out from these dry foils and pressed under 1.5 t/cm^2 for 15 s. Further, the cathode discs were dried at 110 °C under a vacuum oven for 12 h before being transferred to the glovebox for cell assembly. The average loading of the active material was 5–6 mg/cm^2. Using these cathodes, the LNO//Li half-cells were assembled with either commercial LP40 (1 M LiPF6 in EC: DEC 1:1 (v:v) Elyte innovations) or lab-prepared LiFSI-4DME electrolyte, a Li-metal anode circle of 18 mm diameter, and one 20 mm Celgard 2320 separator in between. The assembled half-cells were subjected to galvanostatic charge-discharge tests in the voltage range of 2.8–4.3 V vs Li/Li$^+$ at room temperature. The initial formation process was conducted at 0.1C for 3 cycles, followed by continuous cycling at 0.2C or 1C rate. For full-cells, graphite anode discs (17 mm diameter) were prepared by milling 91 wt.% natural graphite, 5 wt.% Super C65 carbon black, binder comprising of 2 wt.% sodium carboxymethyl cellulose and 2 wt.% styrene-butadiene rubber, and cast on 20 μm-thick copper foils. LNO//graphite full cells were cycled with LiFSI-4DME electrolyte in the potential window 2.5 −4.2 V, and the anode areal capacity was maximized by 10% excess compared to the cathode.

4.1. Online electrochemical mass spectrometry (OEMS)

Electrode preparation: The positive electrodes were prepared based on bare and oMWCNT/PAA (1:3) coated LNO powder (BASF). For this purpose, 0.9 g of LNO powder was mixed with 0.05 g of Super C65 Nano Carbon Black (MSE Supplies) and with a solution of 0.05 g of PVdF Solef® 5130 (Solvay) in N-methyl pyrrolidinone using Ultra Turrax. The positive electrode slurries were cast on an aluminum foil of 20 μm thick using a doctor blade technique. The electrodes were dried in a vacuum at 80 °C for 48 h, then calendered to achieve 35% porosity. The active material loading was 11.1 mg/cm^2 for the bare LNO electrode and 14.1 mg/cm^2 for the oMWCNT/PAA (1:3) coated LNO electrode.

Experimental Set-up: OEMS tests were conducted in a commercial El-cell (ECC-Air) equipped with a gas inlet and outlet. A 15 mm diameter disk of LNO electrode was punched and sandwiched with 2 layers of DreamWeaver Gold separator and with a delithiated LiFePO$_4$ electrode of 16 mm diameter. The latter electrode was delithiated electrochemically in a coin cell versus a Li metal electrode. Further, the coin cell was dismantled, and the retrieved LFP electrode was rinsed with dimethyl carbonate solvent and dried in a vacuum. A loading of the LFP electrode was adjusted to accommodate Li$^+$ ions from LNO electrodes while remaining at a stable voltage of 3.42 V vs Li/Li$^+$ during electrochemical

Table 1

Acronyms of coated LNO samples with varying oMWCNT/PAA composition ratios.

Sample	o-MWCNT (wt.%)	PAA (wt.%)
LNO@oMWCNT/PAA (1:0)	100	0
LNO@oMWCNT/PAA (1:1)	50	50
LNO@oMWCNT/PAA (3:1)	75	25
LNO@oMWCNT/PAA (1:3)	25	75
LNO@oMWCNT/PAA (0:1)	0	100

tests. 1.3 M LiPF$_6$ in ethylene carbonate (EC) electrolyte was used for the OEMS experiments. This basic electrolyte has the advantage of low vapor pressure, which means limited volatility, no risk of mass spectrometer pollution with organic solvents, and no interference with measurements between produced gases and the solvents. 300 µl of the electrolyte was added to the El-cell for each OEMS test. 6 h rest period was applied after the cell assembly and its connection to the gas analysis circuit to allow stabilization of mass spectrometry baseline signals. The typical electrochemical protocol consisted of the following steps at C/10 current: 2 galvanostatic cycles between 4.2 V and 2.5 V vs Li/Li$^+$, 1 cycle between 4.5 V and 2.5 V and 1 cycle between 5.0 V and 2.5 V. For the first three cycles a constant voltage step was applied after reaching an upper cut-off voltage until the current drops to C/50. For the fourth cycle, a constant voltage step was limited by 15 min at 5.0 V. A pause of 2 h 30 min was applied after each discharge to allow a full gas evacuation. A cyclic voltammetry protocol was applied to the freshly prepared El-cell in another set of OEMS experiments. In this case, after an initial pause of 6 h, a voltage ramp of 3 mV/min was applied to the cell between 5.0 and 2.5 V vs Li/Li$^+$ for one cycle.

OEMS test assembly included a simple headspace gas sampling circuit, it is depicted in Fig. S22 [50]. Highly pure argon (6.0) was used as a carrier gas. A precise digital mass flow controller allowed gas supply regulation at 1.2 ml/min to minimize the impact of gas flow on the electrochemical reaction and to limit dilution of the products of the electrochemical reactions. BioLogic SP-300 potentiostat was used for the electrochemical measurements. A Hiden HPR20 S1000 mass spectrometer with ion count detector was employed for continuous online gas monitoring. The following signals were measured in multiple ion detection mode during each test: $m/z = 32$ for O$_2$, $m/z = 44$ for CO$_2$, $m/z = 28$ for CO (the contribution from CO$_2$ to this signal was corrected mathematically using the formula I(28, CO) = $I(28)$ – I(44, CO$_2$)*0.1, where I represents intensity of mass spectrometry signals) and $m/z = 36$ for Ar. After each test, a standard gas mixture (Ar 6.0 with 100 mol ppm of each CO$_2$, CO, and O$_2$ from Air Products) was passed through the gas analysis circuit, allowing conversion of the mass spectrometry ion count signal to molar flux of gases. Integration of signals from each gas at every cycle gave absolute amounts of gases evolved during the electrochemical tests. OEMS experiments were repeated two times to ensure the reproducibility of the results obtained.

CRediT authorship contribution statement

Rekha Narayan: Writing – original draft, Visualization, Methodology, Data curation, Conceptualization. **Irina Profatilova:** Writing – original draft, Visualization, Resources, Methodology, Data curation. **Gregor Kapun:** Formal analysis. **Elena Tchernychova:** Formal analysis. **Elisabeth Addes:** Validation, Supervision. **Robert Dominko:** Writing – review & editing, Supervision, Methodology, Investigation, Funding acquisition, Conceptualization.

Declaration of competing interest

The authors declare that they have no known competing financial interests or personal relationships that could have appeared to influence the work reported in this paper.

for the preparation of the electrodes for OEMS analysis.

Supplementary materials

Supplementary material associated with this article can be found, in the online version, at doi:10.1016/j.ensm.2025.104316.

Data availability

Data will be made available on request.

References

[1] G.T. Park, B. Namkoong, S.B Kim, J. Liu, C.S. Yoon, Y.K Sun, Introducing high-valence elements into cobalt-free layered cathodes for practical lithium-ion batteries, Nat. Energy 7 (10) (2022) 946–954, https://doi.org/10.1038/s41560-022-01106-6.
[2] Y. Luo, H.X. Wei, L. Tang, Y. Huang, Z. Wang, Z. He, C. Yan, J. Mao, K. Dai, J. Zheng, Nickel-rich and cobalt-free layered oxide cathode materials for lithium ion batteries, Energy Storage Mater. 50 (February) (2022) 274–307, https://doi.org/10.1016/j.ensm.2022.05.019.
[3] H.H. Ryu, G.C. Kang, R. Ismoyojati, G.T. Park, F. Maglia, Y.K. Sun, Intrinsic weaknesses of co-free Ni–Mn layered cathodes for electric vehicles, Mater. Today 56 (June) (2022) 8–15, https://doi.org/10.1016/j.mattod.2022.03.005.
[4] C. Wu, R. Li, T. Chen, T. Hu, D. Wang, L. Qiu, B. Zhong, Z. Wu, X. Guo, Understanding of the irreversible phase transition and Zr-doped modification strategy for a Nickel-rich cathode under a high voltage, ACS Sustain. Chem. Eng. 10 (11) (2022) 3651–3660, https://doi.org/10.1021/acssuschemeng.1c08633.
[5] C. Xu, P.J. Reeves, Q. Jacquet, C.P. Grey, Phase Behavior during electrochemical cycling of Ni-Rich cathode materials for Li-ion batteries, Adv. Energy Mater. 11 (7) (2021) 1–12, https://doi.org/10.1002/aenm.202003404.
[6] H.H. Sun, A. Manthiram, Impact of microcrack generation and surface degradation on a Nickel-Rich Layered Li[Ni0.9Co0.05Mn0.05]O2 Cathode for lithium-ion batteries, Chem. Mater. 29 (19) (2017) 8486–8493, https://doi.org/10.1021/acs.chemmater.7b03268.
[7] P. Teichert, G.G. Eshetu, H. Jahnke, E. Figgemeier, Degradation and aging routes of Ni-rich cathode based Li-ion batteries, Batteries 6 (1) (2020) 1–26, https://doi.org/10.3390/batteries6010008.
[8] S.L. Dreyer, A. Kondrakov, J. Janek, T. Brezesinski, In situ analysis of gas evolution in liquid- and solid-electrolyte-based batteries with current and next-generation cathode materials, J. Mater. Res. 37 (19) (2022) 3146–3168, https://doi.org/10.1557/s43578-022-00586-2.
[9] R. Sim, A. Manthiram, Factors influencing gas evolution from high-nickel layered oxide cathodes in lithium-based batteries, Adv. Energy Mater. 14 (8) (2024) 1–13, https://doi.org/10.1002/aenm.202303985.
[10] L. Sören, K.R. Dreyer, Ð.T. Kretschmer, R.C. Andrey Mazilkin, R. Azmi, P. Hartmann, M. Bianchini, T.B. Janek, Multi-Element Surface Coating of Layered Ni-Rich Oxide Cathode Materials and Their.Pdf, Adv. Mater. Interfaces (2022) 9.
[11] C. Liu, Z. Cui, A. Manthiram, Tuning dopant distribution for stabilizing the surface of high-nickel layered oxide cathodes for lithium-ion batteries, Adv. Energy Mater. 14 (3) (2024) 1–14, https://doi.org/10.1002/aenm.202302722.
[12] F. Strauss, J.H. Teo, J. Maibach, A.Y. Kim, A. Mazilkin, J. Janek, T. Brezesinski, Li2ZrO3-Coated NCM622 for application in inorganic solid-state batteries: role of surface carbonates in the cycling performance, ACS Appl. Mater. Interfaces 12 (51) (2020) 57146–57154, https://doi.org/10.1021/acsami.0c18590.
[13] Y. Ma, R. Zhang, Y. Ma, T. Diemant, Y. Tang, S. Payandeh, D. Goonetilleke, D. Kitsche, X. Liu, J. Lin, A. Kondrakov, T. Brezesinski, Interface and electrode microstructure engineering for optimizing performance of the LiNiO2 cathode in all-solid-state batteries, Chem. Mater. 36 (5) (2024) 2588–2598, https://doi.org/10.1021/acs.chemmater.4c00301.
[14] Y. Ma, R. Zhang, Y. Tang, Y. Ma, J.H. Teo, T. Diemant, D. Goonetilleke, J. Janek, M. Bianchini, A. Kondrakov, T. Brezesinski, Single- to few-layer nanoparticle cathode coating for thiophosphate-based all-solid-state batteries, ACS Nano 16 (11) (2022) 18682–18694, https://doi.org/10.1021/acsnano.2c07314.
[15] Y. Ma, J.H. Teo, F. Walther, Y. Ma, R. Zhang, A. Mazilkin, Y. Tang, D. Goonetilleke, J. Janek, M. Bianchini, T. Brezesinski, Advanced nanoparticle coatings for stabilizing layered ni-rich oxide cathodes in solid-state batteries, Adv. Funct. Mater. (23) (2022) 32, https://doi.org/10.1002/adfm.202111829.
[16] H.H. Sun, U.H. Kim, J.H. Park, S.W. Park, D.H. Seo, A. Heller, C.B. Mullins, C. S. Yoon, Y.K. Sun, Transition metal-doped ni-rich layered cathode materials for durable li-ion batteries, Nat. Commun. 12 (1) (2021) 1–11, https://doi.org/10.1038/s41467-021-26815-6.
[17] X. Tan, M. Zhang, J. Li, D. Zhang, Y. Yan, Z. Li, Recent progress in coatings and methods of Ni-Rich LiNi0.8Co0.1Mn0.1O2 cathode materials: a short review, Ceram. Int. 46 (14) (2020) 21888–21901, https://doi.org/10.1016/j.ceramint.2020.06.091.
[18] N.S. Luu, P.E. Meza, A.M. Tayamen, O. Kahvecioglu, S.V. Rangnekar, J. Hui, J. R. Downing, M.C. Hersam, Enabling ambient stability of LiNiO2 lithium-ion battery cathode materials via graphene-cellulose composite coatings, Chem. Mater. 35 (13) (2023) 5150–5159, https://doi.org/10.1021/acs.chemmater.3c00851.
[19] L. Wang, A. Mukherjee, C.Y. Kuo, S. Chakrabarty, R. Yemini, A.A. Dameron, J. W. DuMont, S.H. Akella, A. Saha, S. Taragin, H. Aviv, D. Naveh, D. Sharon, T.

S. Chan, H.J. Lin, J.F. Lee, C.T. Chen, B. Liu, X. Gao, S. Basu, Z. Hu, D. Aurbach, P. G. Bruce, M. Noked, High-energy all-solid-state lithium batteries enabled by Co-Free LiNiO2 cathodes with robust outside-in structures, Nat. Nanotechnol. 19 (2) (2024) 208–218, https://doi.org/10.1038/s41565-023-01519-8.

[20] Chu Y., Zhou J., Liu W., Chu F., Li J.. Cobalt-free LiNiO 2 with a selenium coating as a high-energy layered cathode material for lithium-ion batteries. *Small Sci.* 3, 2300023.

[21] P. Guan, L. Zhou, Z. Yu, Y. Sun, Y. Liu, F. Wu, Y. Jiang, D. Chu, Recent progress of surface coating on cathode materials for high-performance lithium-ion batteries, J. Energy Chem. 43 (2020) 220–235, https://doi.org/10.1016/j.jechem.2019.08.022.

[22] X. Wan, T. Mu, B. Shen, Q. Meng, G. Lu, S. Lou, P. Zuo, Y. Ma, C. Du, G. Yin, Stable silicon anodes realized by multifunctional dynamic cross-linking structure with self-healing chemistry and enhanced ionic conductivity for lithium-ion batteries, Nano Energy 99 (March) (2022) 107334, https://doi.org/10.1016/j.nanoen.2022.107334.

[23] W. Zhu, J. Zhou, S. Xiang, X. Bian, J. Yin, J. Jiang, L. Yang, Progress of binder structures in silicon-based anodes for advanced lithium-ion batteries: a mini review, Front. Chem. 9 (October) (2021) 1–11, https://doi.org/10.3389/fchem.2021.712225.

[24] J.-H. Kuo, C.-C. Li, Water-based process to the preparation of Nickel-Rich Li(Ni 0.8 Co 0.1 Mn 0.1)O 2 cathode, J. Electrochem. Soc. 167 (10) (2020) 100504, https://doi.org/10.1149/1945-7111/ab95c5.

[25] G. Hu, J. Fan, Y. Lu, Y. Zhang, K. Du, Z. Peng, L. Li, B. Zhang, Y. Shi, Y. Cao, Surface architecture design of LiNi0.8Co0.15Al0.05O2 cathode with synergistic organics encapsulation to enhance electrochemical stability, ChemSusChem 13 (21) (2020) 5699–5710, https://doi.org/10.1002/cssc.202001771.

[26] S. Peng, X. Kong, J. Li, J. Zeng, J. Zhao, Alleviating the Storage Instability of LiNi0.8Co0.1Mn0.1O2Cathode Materials by Surface Modification with Poly (Acrylic Acid), ACS Sustain. Chem. Eng. 9 (22) (2021) 7466–7478, https://doi.org/10.1021/acssuschemeng.1c00802.

[27] R. Shunmugasundaram, R. Senthil Arumugam, P. Benedek, M. Yarema, P. Baade, V. Wood, In situ formation of lithium polyacrylate binder for aqueous manufacturing and recycling of Ni-Rich cathodes, J. Electrochem. Soc. 169 (6) (2022) 060504, https://doi.org/10.1149/1945-7111/ac7171.

[28] H. Gao, Y. Meng, X. Liu, F. Zhu, Improvement of electrochemical properties of LiCoO2 at 4.6 V by a LiPAA coating, J. Mater. Sci. Mater. Electron. 33 (21) (2022) 17125–17136, https://doi.org/10.1007/s10854-022-08588-w.

[29] J. Yang, P. Li, F. Zhong, X. Feng, W. Chen, X. Ai, H. Yang, D. Xia, Y. Cao, Suppressing voltage fading of li-rich oxide cathode via building a well-protected and partially-protonated surface by polyacrylic acid binder for cycle-stable Li-Ion batteries, Adv. Energy Mater. 10 (15) (2020) 1–10, https://doi.org/10.1002/aenm.201904264.

[30] K.A. Hays, R.E. Ruther, A.J. Kukay, P. Cao, T. Saito, D.L. Wood, J. Li, What makes lithium substituted polyacrylic acid a better binder than polyacrylic acid for silicon-graphite composite anodes? J. Power Sources 384 (March) (2018) 136–144, https://doi.org/10.1016/j.jpowsour.2018.02.085.

[31] G.V. Zhuang, G. Chen, J. Shim, X. Song, P.N. Ross, T.J. Richardson, Li2CO3 in LiNi0.8Co0.15Al 0.05O2 cathodes and its effects on capacity and power, J. Power Sources 134 (2) (2004) 293–297, https://doi.org/10.1016/j.jpowsour.2004.02.030.

[32] S. Chen, T. He, Y. Su, Y. Lu, L. Bao, L. Chen, Q. Zhang, J. Wang, R. Chen, F. Wu, Ni-Rich LiNi0.8Co0.1Mn0.1O2 oxide coated by dual-conductive layers as high performance cathode material for lithium-ion batteries, ACS Appl. Mater. Interfaces 9 (35) (2017) 29732–29743, https://doi.org/10.1021/acsami.7b08006.

[33] W. Gu, Q. Dong, L. Zheng, Y. Liu, Y. Mao, Y. Zhao, W. Duan, H. Lin, Y. Shen, L. Chen, Ambient air stable Ni-rich layered oxides enabled by hydrophobic self-assembled monolayer, ACS Appl. Mater. Interfaces 12 (1) (2020) 1937–1943, https://doi.org/10.1021/acsami.9b20030.

[34] L. Baggetto, N.J. Dudney, G.M. Veith, Surface chemistry of metal oxide coated lithium manganese nickel oxide thin film cathodes studied by XPS, Electrochim. Acta 90 (2013) 135–147, https://doi.org/10.1016/j.electacta.2012.11.120.

[35] Y.S. Wu, Q.T. Pham, C.C. Yang, C.S. Chern, L. Musuvadhi Babulal, M. Seenivasan, G. Brunklaus, T. Placke, B.J. Hwang, M. Winter, Study of electrochemical performance and thermal property of LiNi0.5Co0.2Mn0.3O2 cathode materials

[36] Y. Ding, B. Deng, H. Wang, X. Li, T. Chen, X. Yan, Q. Wan, M. Qu, G. Peng, Improved electrochemical performances of LiNi0.6Co0.2Mn0.2O2 cathode material by reducing lithium residues with the coating of prussian blue, J. Alloys Compd. 774 (2019) 451–460, https://doi.org/10.1016/j.jallcom.2018.09.286.

[37] C. Busà, M. Belekoukia, M.J. Loveridge, The effects of ambient storage conditions on the structural and electrochemical properties of NMC-811 cathodes for Li-Ion batteries, Electrochim. Acta (2021) 366, https://doi.org/10.1016/j.electacta.2020.137358.

[38] N. Li, Y. Shi, Y. Yin, X. Zeng, J. Li, C. Li, L. Wan, R. Wen, Y. Guo, Inside cover: a flexible solid electrolyte interphase layer for long-life lithium metal anodes (Angew. Chem. Int. Ed. 6/2018), Angew. Chemie Int. Ed. 57 (6) (2018) 1422, https://doi.org/10.1002/anie.201713193. –1422.

[39] J. Kasnatscheew, M. Evertz, B. Streipert, R. Wagner, R. Klöpsch, B. Vortmann, H. Hahn, S. Nowak, M. Amereller, A.C. Gentschev, P. Lamp, M. Winter, The Truth about the 1st cycle coulombic efficiency of LiNi1/3Co1/3Mn1/3O2 (NCM) Cathodes, Phys. Chem. Chem. Phys. 18 (5) (2016) 3956–3965, https://doi.org/10.1039/c5cp07718d.

[40] J. Qian, W.A. Henderson, W. Xu, P. Bhattacharya, M. Engelhard, O. Borodin, J. G. Zhang, High rate and stable cycling of lithium metal anode, Nat. Commun. (2015) 6, https://doi.org/10.1038/ncomms7362.

[41] X. Ren, L. Zou, S. Jiao, D. Mei, M.H. Engelhard, Q. Li, H. Lee, C. Niu, B.D. Adams, C. Wang, J. Liu, J.G. Zhang, W. Xu, High-concentration ether electrolytes for stable high-voltage lithium metal batteries, ACS Energy Lett 4 (4) (2019) 896–902, https://doi.org/10.1021/acsenergylett.9b00381.

[42] Täubert, C.; Fleischhammer, M.; Wohlfahrt-mehrens, M.; Li, J.; Harlow, J.; Stakheiko, N.; Zhang, N.; Paulsen, J.; Dahn, J. Dependence of cell failure on cut-off voltage ranges and observation of kinetic hindrance in dependence of cell failure on cut-off voltage ranges and observation of kinetic hindrance in LiNi 0 . 8 Co 0 . 15 Al 0 . 05 O 2. https://doi.org/10.1149/2.0491811jes.

[43] C.R. Birkl, M.R. Roberts, E. Mcturk, P.G. Bruce, D.A. Howey, Degradation diagnostics for lithium ion cells, J. Power Sources 341 (2017) 373–386, https://doi.org/10.1016/j.jpowsour.2016.12.011.

[44] Jung, R.; Morasch, R.; Karayaylali, P.; Phillips, K.; Maglia, F.; Stinner, C.; Shao-horn, Y.; Gasteiger, H.A. Effect of ambient storage on the degradation of Ni-rich positive electrode materials (NMC811) for Li-ion batteries effect of ambient storage on the degradation of Ni-rich positive electrode materials (NMC811) for Li-ion batteries. https://doi.org/10.1149/2.0401802jes.

[45] S.E. Renfrew, B.D. McCloskey, Residual lithium carbonate predominantly accounts for first Cycle CO2 and CO outgassing of Li-stoichiometric and Li-rich layered transition-metal oxides, J. Am. Chem. Soc. 139 (49) (2017) 17853–17860, https://doi.org/10.1021/jacs.7b08461.

[46] R. Jung, M. Metzger, F. Maglia, C. Stinner, H.A. Gasteiger, Oxygen release and its effect on the cycling stability of LiNi x Mn y Co z O 2 (NMC) Cathode materials for Li-ion batteries, J. Electrochem. Soc. 164 (7) (2017) A1361–A1377, https://doi.org/10.1149/2.0021707jes.

[47] L. de Biasi, A. Schiele, M. Roca-Ayats, G. Garcia, T. Brezesinski, P. Hartmann, J. Janek, Phase transformation behavior and stability of LiNiO2 cathode material for Li-ion batteries obtained from in situ gas analysis and operando X-ray diffraction, ChemSusChem 12 (10) (2019) 2240–2250, https://doi.org/10.1002/cssc.201900032.

[48] Z. Cui, A. Manthiram, Thermal stability and outgassing behaviors of high-nickel cathodes in lithium-ion batteries, Angew. Chemie - Int. Ed 62 (43) (2023), https://doi.org/10.1002/anie.202307243.

[49] G. Zhang, Y. Zhu, S. Lv, Z. Wang, P. Gao, Enhanced electrochemical performance of LiNiO2 cathode material by precursor preoxidation for lithium-ion batteries, J. Alloys Compd. 953 (2023) 170134, https://doi.org/10.1016/j.jallcom.2023.170134.

[50] B. Rajagopalan, M. Pichardo, I. de Meatza, I. Profatilova, U. Osa, S. Sananes-Israel, E. Paillard, An ethylene carbonate/propylene carbonate electrolyte for improved cycle life and safety of silicon-graphite/NMC (Ni = 80–83 %) high-energy lithium-ion battery cells, J. Power Sources 2025 (October 2024) 627, https://doi.org/10.1016/j.jpowsour.2024.235778.